

Assessing the robustness of amortized simulation-based inference to transient noise in gravitational-wave ringdowns

Song-Tao Liu,¹ Tian-Yang Sun,¹ Yu-Xin Wang,¹ Yong-Xin Zhang,¹ Shang-Jie Jin,¹ Jing-Fei Zhang,¹ and Xin Zhang^{1,2,3,*}

¹*Liaoning Key Laboratory of Cosmology and Astrophysics,
College of Sciences, Northeastern University, Shenyang 110819, China*

²*MOE Key Laboratory of Data Analytics and Optimization for Smart Industry,
Northeastern University, Shenyang 110819, China*

³*National Frontiers Science Center for Industrial Intelligence and Systems Optimization,
Northeastern University, Shenyang 110819, China*

Gravitational waves (GW) emitted by binary systems allow us to perform precision tests of general relativity in the strong field regime. Ringdown signals allow for probing black hole mass and spin with high precision in GW astronomy. With improvements in current and next-generation GW detectors, developing likelihood-free parameter inference methods is crucial. This is especially important when facing challenges such as non-standard noise, partial data, or incomplete signal models that prevent the use of analytical likelihood functions. In this work, we propose an amortized simulation-based inference strategy to estimate ringdown parameters directly. Specifically, our method is based on amortized neural posterior estimation, which trains a neural density estimator of the posterior for all data segments within the prior range. The results show that our trained amortized network achieves statistically consistent parameter estimates with valid confidence coverage compared to established Markov-chain methods, while offering inference speeds that are orders of magnitude faster. Furthermore, we evaluate the robustness of the method against transient noise contamination. Our analysis reveals that the timing of glitch injection has a decisive impact on estimation bias, particularly during the tail of a signal with sparse information. Glitch strength is positively correlated with estimation error, but has limited effect at low signal-to-noise ratios. Mass and spin parameters are most sensitive to noise. This study not only provides an efficient and accurate inference framework for ringdown analysis but also lays a foundation for developing robust data-processing pipelines for future GW astronomy in realistic noise environments.

I. INTRODUCTION

Gravitational waves (GW) were directly detected for the first time in 2015. The signal GW150914, which came from binary black holes merging, was discovered by LIGO [1]. Since then, GW astronomy has grown quickly. A growing number of GW events have been observed, including binary black hole mergers, binary neutron star mergers, and black hole-neutron star mergers [2–6]. A global detector network including LIGO, Virgo, and KAGRA has observed dozens of GW events. These observations strongly support Einstein’s theory of general relativity. These observations also provide valuable insights into astrophysics, fundamental physics, and cosmology [7–17]. The ringdown phase of GW constitutes a crucial component of the GW signal emitted following the merger of compact objects, such as black holes or neutron stars [1]. Physically, this stage corresponds to the transition of the newly formed black hole toward a stable Kerr black hole state [7]. During this process, the remaining black holes are strongly perturbed and radiate GW to dissipate its initial energy and angular momentum, ultimately reach a stationary configuration [18].

Within the cosmological framework, general relativity

serves as the cornerstone theory describing the evolution of large-scale structure, while the GW ringdown stage provides an experimental platform for testing this theory under extreme conditions [19]. The characteristic signals of quasi-normal modes (QNM) [20] emitted during the ringdown phase are entirely determined by the mass and spin parameters of the newly formed black hole, allowing their frequency and damping rate to be used as precision tests of general relativity [18, 21]. The ringdown signal can also serve as a standard measurement tool, providing an independent avenue for constraining cosmological parameters [8, 22–27]. The measured QNM frequencies can calibrate the mass and spin of the final black hole, while these oscillation modes are closely linked to redshift effects [28]. Consequently, observing the ringdown signals from distant black hole merger events can place constraints on cosmological parameters such as the Hubble constant, the dark energy equation of state, and so on in broader cosmological models [29–44]. For example, the temporal evolution of ringdown data, combined with detectors of extremely high relative precision, such as Laser Interferometer Space Antenna (LISA) [34, 45] or third-generation GW observatories, offers a potential method for improving cosmic distance measurement [27, 46]. Moreover, this approach allows for the construction of a cosmological black-hole population model through “event by event” detection, which can be used to study structure formation processes in the

* Corresponding author.
zhangxin@mail.neu.edu.cn

early universe [47, 48]. Furthermore, certain cosmological theories, such as dark energy models [42, 49, 50] or scalar-tensor gravity [19, 51, 52], may affect the speed and modal characteristics of GW propagation. By precisely measuring the QNM frequencies of the ringdown signal, it becomes possible to constrain the parameter space of such theories or test their validity.

However, GW astronomy is still in the early stages. The available data are limited, and detector sensitivity remains insufficient [53]. Progress depends on better theoretical models, and numerical simulations are a key tool in developing them [54–58]. Currently, traditional likelihood-based methods exhibit several limitations in the face of non-standard noise, partial data, and incomplete signal modeling [59–61]. Firstly, traditional likelihood methods typically assume that the noise is Gaussian, white, and stationary, which simplifies the computation of the likelihood function [62–64]. However, actual GW detector data often contain non-Gaussian and non-stationary noise components, such as glitches [65–69]. When noise characteristics deviate from these ideal assumptions, likelihood functions based on a Gaussian noise model may fail to accurately describe the data, leading to biased or inaccurate parameter estimates [70]. Secondly, in some observational scenarios, only partial data may be available, or the data may contain gaps [71, 72]. Traditional likelihood-based approaches can struggle to handle incomplete datasets, often requiring complex processing or interpolation techniques that may introduce additional errors or uncertainties [73]. Finally, accurate modeling of GW signals, particularly for strong field events such as black hole mergers, remains a challenging task [54]. If the signal model is incomplete or inaccurate, for example by omitting significant QNM, even an accurate noise model may fail to infer the physical parameters correctly [74].

Due to the low event rate detected by current GW detectors, existing sequential neural network approaches have so far been limited to testing only the signal of an event [75–78]. However, with the advancement of GW detection technology, the next generation of GW detectors, including proposed detectors such as LISA, the Einstein Telescope (ET) [79], and Cosmic Explorer (CE) [80, 81] will represent a revolutionary advance. The most fundamental and transformative improvement is the exponential increase in event rates [82]. Compared to the current joint observations by LIGO/Virgo/KAGRA, which detect dozens of compact binary coalescence events per year, next-generation facilities will increase the observable event rate to thousands or even tens of thousands annually. Therefore, it is very crucial to find an efficient parameter estimation method to deal with a large number of events [22, 83–85].

Deep learning has garnered significant attention due to its successful application in GW detection [58, 63, 83, 86–99]. To overcome the computational limitations of traditional methods, researchers have begun exploring alternative approaches using deep learning to address these

challenges. Neural Posterior Estimation (NPE) has emerged as a transformative approach within Simulation-Based Inference (SBI) [100–103], offering a powerful alternative to traditional Bayesian methods for parameter estimation in complex scientific domains. Its development and application to GW astronomy [104–107], particularly for ringdown analysis [78], represent a significant advancement in computational astrophysics [108]. NPE employing a deep learning-based variational autoencoder [109–111], takes advantage of the universal approximation capabilities of neural networks to directly learn a mapping from observed data to an approximate posterior distribution over model parameters, bypassing the need for an explicit, tractable likelihood function [112, 113]. This is especially advantageous in scenarios where the likelihood is intractable due to complex noise properties, incomplete signal models, or high-dimensional parameter spaces. The foundational concept of NPE is rooted in the broader field of SBI, also known as likelihood-free inference. In this paradigm, a simulator, a forward model that can generate synthetic data given a set of parameters, is used to create a large training dataset of input parameters and corresponding simulated observations. A neural network, often a conditional density estimator like a Mixture Density Network or a Normalizing Flow model, is then trained on this dataset to invert the simulator, effectively learning the posterior distribution. Once trained, this neural network can perform inference on new, real observational data in a fraction of the time required by traditional sampling-based methods like Markov Chain Monte Carlo (MCMC) [114]. This speed-up is crucial for the era of big data in astronomy, where facilities like the Vera C. Rubin Observatory and next-generation gravitational wave detectors are expected to produce vast volumes of data.

Moreover, in the presence of non-Gaussian noise, inference using simple neural networks suffers from inherent limitations. Due to their limited robustness, such models may introduce significant bias when approximating the posterior distribution, particularly in the estimation of marginal parameter distributions and joint credible regions [101, 115]. To address this challenge, we developed and evaluated a deep learning framework based on amortized NPE for the rapid and accurate parameter estimation from GW ringdown signals contaminated by non-Gaussian noise. We propose an enhanced amortized NPE architecture featuring increased model complexity to improve the robustness of amortized inference [85]. Specifically, our network is built upon a multi-layer perceptron augmented with residual connections [116], forming an embedding-enhanced NPE estimator. The input data are first compressed into a low-dimensional latent representation via a residual connections embedding network. This compact embedding is then fed into highly flexible Normalizing Flows, specifically, a Neural Spline Flow (NSF), to enable expressive posterior approximation. This design significantly enhances the overall robustness of the inference pipeline. Crucially, the proposed NPE model

undergoes rigorous statistical validation. We assess the calibration of posterior estimates using Monte Carlo coverage tests [117] and further evaluate their statistical consistency by applying the Kolmogorov-Smirnov (KS) test [118] on a test set. Additionally, we test the model's performance on data contaminated with realistic glitches and quantify its robustness by computing the Jensen-Shannon Divergence (JSD) between posterior estimates from glitch-contaminated and clean (noise-free) signals.

This paper is organized as follows. In Section II we introduce the amortized NPE method, the ringdown waveform model, the data generation and training process, and the statistical tests used for model evaluation. Section III presents the calibration performance of the model on clean data and systematically analyzes the impact of transient noise, i.e., glitches on inference results. Finally, Section IV summarizes the main findings and outlines future research directions.

II. METHODOLOGY

A. Amortized NPE

Amortized NPE commonly employs Normalizing Flow [119, 120] as density estimators [121, 122]. Normalizing flow uses an invertible bijective transformation f to map a complex target distribution to a simple base distribution $\varpi(\mathbf{z})$ that is fast to evaluate. For amortized NPE, the target distribution is $p(\boldsymbol{\theta}|\mathbf{x})$ and $\varpi(\mathbf{z})$ which is typically a simple base distribution. The transformation $f: \mathbf{z} \rightarrow \boldsymbol{\theta}$ must be invertible and have a tractable Jacobian. This is so that we can evaluate the target distribution from $\varpi(\mathbf{z})$ by a change of variable:

$$p(\boldsymbol{\theta}|\mathbf{x}) = \varpi(\mathbf{z}) \left| \det \left(\frac{\partial f^{-1}}{\partial \boldsymbol{\theta}} \right) \right|. \quad (1)$$

The goal of amortized NPE is to estimate the posterior density over the entire prior volume covered by the training set. This means it trains a single neural network model that can estimate the full posterior distribution for any observed data drawn from the same prior distribution, without the need for retraining or performing inference anew for each individual observation.

We use amortized NPE to estimate posterior densities. Amortized NPE was introduced in [123, 124] and further expanded in astrophysics [125, 126]. The aim of amortized NPE is training an approximate density estimator $q_\phi(\boldsymbol{\theta}|\mathbf{x})$ of the posterior density $p(\boldsymbol{\theta}|\mathbf{x})$. Here \mathbf{x} is the data segment and $\boldsymbol{\theta}$ is the set of model parameters to be estimated; to be more precise, \mathbf{x} is the sum of a simulated ringdown waveform data $\mathbf{h}(\boldsymbol{\theta})$ which is deterministic component and a stochastic component \mathbf{n} (the noise of detector), i.e. $\mathbf{x}(\boldsymbol{\theta}) = \mathbf{h}(\boldsymbol{\theta}) + \mathbf{n}$. In brief, we generate $\mathbf{h}(\boldsymbol{\theta})$ through a numerical process, so as to prepare a training set of paired samples $\{\boldsymbol{\theta}_i, \mathbf{x}_i\}$ to train the density estimator.

The training process maximizes the likelihood $\prod_i q_\phi(\boldsymbol{\theta}|\mathbf{x}_i)$ with respect to the model parameters ϕ . The estimator asymptotically converges to the true posterior density as the size of the training set increases. As mentioned above our estimator used NSF [113], spline-based neural normalizing flows. Once trained, the estimator q_ϕ can be sampled from within a few seconds, returning a set of posterior samples $\{\boldsymbol{\theta}_n\}$.

B. Ringdown waveform

The form of the GW strain can be expressed by

$$\mathbf{h}(\boldsymbol{\theta}) = F_+ h_+ + F_\times h_\times. \quad (2)$$

Here F_+ and F_\times are the pattern functions of the detector [127], depending on the sky position and relative orientation of the source, the polarization angle of the waveform and the starting time of the ringdown.

The plus mode and cross mode waveform are expressed as superpositions of damped sinusoids as

$$h_+ = \sum_{l,m,n} \mathcal{A}_{lmn} e^{-\frac{(t-t_{\text{start}})}{\tau_{lmn}}} \cos(\Phi_{lmn}) Y_{lm}^+(\iota), \quad (3a)$$

$$h_\times = \sum_{l,m,n} \mathcal{A}_{lmn} e^{-\frac{(t-t_{\text{start}})}{\tau_{lmn}}} \sin(\Phi_{lmn}) Y_{lm}^\times(\iota). \quad (3b)$$

For parameter estimation, we fix the sky position, polarization, starting time, and inclination as known parameters.

C. Data generation and training

We perform data generation with only detector noise to test the ability to recover a set of known injection parameters. We simulate the simplest harmonic superposition model: $Kerr_{2,2,0}$, a system containing only the (2, 2, 0) mode.

For convenience, we adopt the same right ascension α , declination δ , and polarization ψ parameters as those of the GW150914-like event, and fix the inclination angle at $\iota = \pi$ [74, 128]. The noise is randomly generated from the designed power spectral density (PSD) of aLIGO. For the simulated injections, we sample the strains at 2048 Hz and truncate the waveform to a duration of 0.1 seconds, thus resulting in a data segment of 204 bins. All ringdown signals are simulated for a single detector (LIGO-Hanford).

We model the density estimator as an NSF [129] and use the implementation from the `lampe` package. The relevant hyper-parameters are listed in Table I. In particular, the NSF is a flow of 5 transforms and 4 hidden features, each with 128 units.

The NSF does not directly feed whitened data into the network for training. Instead, an embedding network is applied for dimensionality reduction: the simulated single-detector input is first up-sampled to twice its original dimension. The data are then mapped by a fully connected neural network to 128 bins, further compressed to 64 bins, and finally the compressed data are passed to the NSF for inference. This network follows an "expand then compress" strategy, consisting of three hidden layers. Each layer is equipped with layer normalization and dropout regularization to enhance training stability.

Subsequently, this embedded representation is used as a conditional input to a posterior estimator based on NSF. Here, five stacked spline-coupling layers perform invertible transformations modulated by corresponding conditional networks. The final output is the posterior probability density of the target parameters.

We train and evaluate the density estimator on a batch of 4096 samples. In each round of training we generate 50000 training samples. We use the Adam optimizer with a learning rate of 0.001. We train the posterior density estimators on a single GPU RTX A6000. The training processes take 100 epochs and last 9.6 hours.

TABLE I. The key hyperparameters of the amortized NPE.

NSF	
hidden features	128
transforms	5
Activation	ReLU
Batch Norm	False
Embedding network	
input dimension	408
hidden layers	3
hidden dimension	[200, 100, 128]
output dimension	64
Training hyper-parameters	
number of simulations	50000
batch size	4096
learning rate	0.001
patience	50
varying noise	TRUE

We evaluate the amortized NPE method using test data of simulated ringdown signals. For this test, the mass and spin of the remnant black hole are fixed to $\mathcal{M}_f = 67M_\odot$ and $\chi_f = 0.67$. To simulate realistic detection conditions comparable to observed events, we target a signal-to-noise ratio (SNR) ≈ 3.5 . This target SNR is achieved by setting the amplitude of the fundamental mode to $\mathcal{A}_{220} = 0.2 \times 10^{-21}$ within the corresponding noise PSD of the detector.

We draw posterior inferences using box-uniform priors on the model parameters, with the prior ranges listed in Table II. We benchmark our results against posterior

samples obtained with the time-domain inference software `pyRing` (v2.3.0) [130–133]. We sample with the nested sampler `cpnest`, using 4096 live points and 4094 maximum Markov-chain steps, which typically results in about 20000 posterior samples. For consistency, we also extract 20000 posterior samples from the trained estimator when doing the comparisons.

TABLE II. Priors of simulated ringdown waveform parameters. Note that other parameters not mentioned are set to zero for simplicity.

Parameter	Uniform distribution
Total mass	$\mathcal{M}_f \in [20, 300] M_\odot$
Spin	$\chi_f \in [0, 0.99]$
Amplitude	$\mathcal{A}_{220} \in [0.1, 50] \times 10^{-21}$
Phase	$\phi_{220} \in [0, 2\pi]$

D. Analytical method

The KS test [134] is a statistical method used to assess the quality of fit between a sample distribution and a reference distribution. In GW ringdown parameter estimation, the KS test can evaluate the consistency between the posterior distribution of parameters and a theoretical or predictive distribution [135–139]. The test first calculates the cumulative distribution functions (CDF) of the two distributions. It then computes the distance D_n between the two distributions based on the CDF, which can be written as

$$D_n = \max |F_n(x) - F(x)|, \quad (4)$$

where $F_n(x)$ is a specified continuous distribution function obtained from a random sample X_1, X_2, \dots, X_n . and $F(x)$ respectively represent the CDF of the two distributions under validation. where is the empirical cumulative distribution function obtained from a random sample, and is the theoretical cumulative distribution function. The resulting D_n is also known as the KS statistic. The p-value, calculated based on the KS statistic, is generally employed as a direct measure to evaluate the similarity or difference between two distributions. The p-value is commonly compared to the significance level. To be specific, if the p-value is less than the significance level, it indicates that the two distributions are considered statistically different. Here, the significance level is set to a value of 0.05.

In our work, we compare the distribution of measured coverage probabilities against the theoretically expected uniform distribution to assess the calibration of the amortized NPE model. It can be shown [140, 141] that, if the distribution generated by our model approximates the true posterior, then the expected coverage is distributed uniformly within $[0, 1]$, which is a uniform distribution. To assess the calibration of the model, we computed the

coverage probability for a representative event in our dataset. Specifically, we drew 200 posterior samples from the model for this event and calculated the fraction of samples that fell below the event’s true parameter value. The null hypothesis is that this distribution is uniform, which would indicate that the posterior inference is statistically consistent. We assess the hypothesis using the KS test, rejecting the null hypothesis at the 5% significance level if $p \leq 0.05$.

The JSD quantifies the difference between two probability distributions and measures the similarity of two distributions [142, 143]. It is achieved by taking a weighted average of the probability density functions of the two distributions, given by

$$\text{JSD}(p \parallel q) = \frac{1}{2} \text{KLD}(p \parallel \frac{p+q}{2}) + \frac{1}{2} \text{KLD}(q \parallel \frac{p+q}{2}), \quad (5)$$

where Kullback-Leibler divergence (KLD) [144, 145] is defined as

$$\text{KLD}(p \parallel q) = \int_{-\infty}^{+\infty} p(x) \ln \frac{p(x)}{q(x)} dx. \quad (6)$$

While the KLD can measure the difference between two probability distributions, it is asymmetric because the KLD between distributions p and q is not equal to that between q and p . To overcome this asymmetry, we employ the JSD, which provides a symmetric and smoothed measure. The JSD is bounded between 0 and 1, where 0 indicates identical distributions and 1 corresponds to maximal dissimilarity [146]. This bounded range facilitates the interpretation and comparison of distributional differences. In this work, we use the JSD to quantify the discrepancy between the parameter posterior inferred by the amortized NPE model from data contaminated with glitches and the ideal posterior.

III. RESULTS AND DISCUSSION

A. Amortized NPE model evaluation

Before assessing the model’s robustness against glitches, we first evaluate the accuracy of the amortized NPE model using data free of non-stationary noise. In this section, we systematically evaluate the performance of the amortized NPE model for parameter inference of GW ringdown signals without glitches through numerical experiments. To investigate how training epochs affect the prediction credibility of the amortized NPE, we compare models trained for a small number of epochs against those trained for a large number, evaluating their posterior coverage across multiple credible intervals.

With limited training, the model initially learns the basic structure of the posterior distribution. Compared to the results from traditional nested sampling, the central tendencies of the key parameter posterior distributions inferred by the model are largely consistent. However,

slight deviations exist in the inferred confidence intervals. The left panel of Fig. 1 compares parameter estimates and confidence intervals from MCMC and amortized NPE, showing a slight mismatch in the inferred credible regions across different confidence levels.

After sufficient training, model performance improves significantly. The posterior distributions it infers show high visual agreement with MCMC results, and divergence measures quantified by the KS test drop to very low levels ($p \geq 0.05$). The results are shown in the right panel of Fig. 1. This demonstrates that a well-trained amortized NPE model produces posterior distributions that are statistically consistent with high-precision MCMC results. At the same time, it achieves inference speed-ups of several orders of magnitude.

As internal diagnostics, we further quantify the statistical reliability of the uncertainty estimates through coverage probability tests. The expected coverage distributions for both training processes are summarized in Fig. 2.

For the low-epoch model, the empirical expected coverage significantly deviates from the ideal line, particularly in the tails. Consequently, the distribution fails the KS test. This indicates that the model is not fully calibrated, and its posterior uncertainties may be either underestimated or overestimated. In contrast, the high-epoch model shows nearly ideal calibration. Its expected coverage closely follows the diagonal reference line, and the corresponding p-values are statistically indistinguishable from a uniform distribution. This demonstrates that the well-trained model can provide reliable estimates, and the confidence intervals it produces are trustworthy.

B. Influence of glitches on model

Non-Gaussian noise refers to a class of noise processes whose statistical distribution deviates from the Gaussian or normal probability model. This noise exhibits more complex statistical characteristics and generative mechanisms, which can significantly compromise the stability of the system, degrade the accuracy of the inference, and reduce the analytical efficiency. In high-precision observational fields like GW astronomy and astrophysical data analysis, non-Gaussian noise, especially glitches, poses a major practical challenge. It directly compromises data interpretability and undermines the reliability of scientific conclusions.

In this chapter, we evaluate the effect of non-Gaussian noise (glitches) on the posterior distribution of model evaluation at different time points and for different SNR of the signal. To assess the robustness of the inference pipeline, we inject simulated glitches into ringdown signals and analyze the resulting biases in the posterior distributions. The following presents our results of glitch injection and the key findings on model performance degradation.

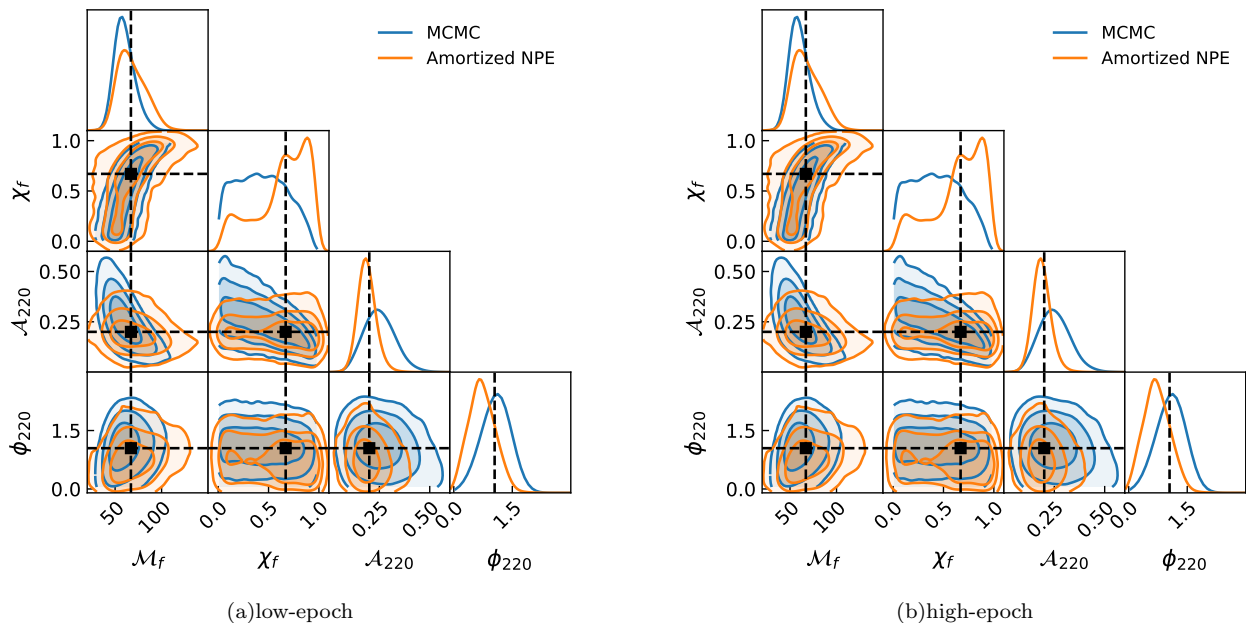


FIG. 1. Comparison of parameter estimates and confidence intervals derived from MCMC and amortized NPE. The figure shows the mean values for parameters \mathcal{M}_f , χ_f , \mathcal{A}_{220} , and ϕ_{220} under the two methods, alongside their 68.3%, 95.5%, and 99.7% credible intervals from the full posterior distribution. The black line marks the values of the injection parameters.

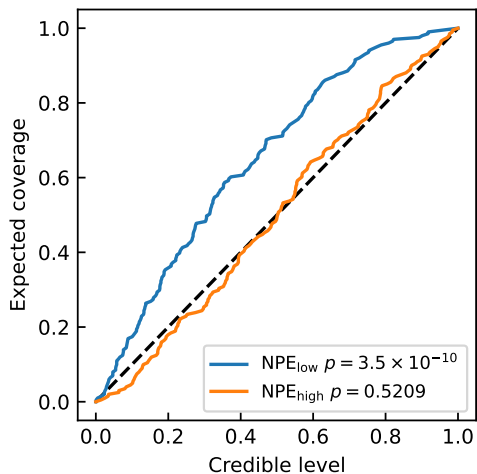


FIG. 2. The figure illustrates the relationship between credible level and expected coverage for models trained under different training epochs. The blue curve represents the 100 epochs training model while the yellow curve corresponds to the 200 epochs model, trained for a higher number of epochs.

1. The time point of glitches

In this section, we assess the impact of glitch injection time on model reliability by measuring the JSD value between the posterior distribution. For convenience, we choose glitches with $\text{SNR} = 14$ for non-Gaussian noise injection. Figure 3 quantifies how the timing of glitch

injection affects the reliability of parameter inference. We measure this impact using the JSD, a symmetric and bounded metric for distributional discrepancy. Here, a JSD value of 0 indicates identical posterior distributions, while larger values correspond to greater deviation.

The curve reveals a pronounced peak in JSD when the glitch is injected after 0.015 seconds, especially in the tail part. This indicates that glitches occurring during this phase of the ringdown signal cause the largest bias in parameter estimation.

This phenomenon can be attributed to the information content of the ringdown signal, which varies over time. The early portion of the ringdown is dominated by the strong emission of the fundamental mode, which carries most of the energy and is relatively robust to localized perturbations. In contrast, the tail portion corresponds to the late time decay of the signal, where higher order modes and noise-dominated segments become more influential. Significant impact occurs only at specific time offsets and when the glitch is out of phase with the signal. This phase alignment enables interference in the time-frequency domain, altering the SNR distribution and degrading localization [147].

When a glitch is injected during this low-amplitude, information-poor phase, it can severely distort the inferred damping rates and mode amplitudes. This distortion, in turn, leads to significant biases in the estimates of mass and spin.

We also assess JSD using marginal distribution as shown in Fig. 4 below. The marginal distributions of mass, spin and amplitude, as well as overall JSD trends

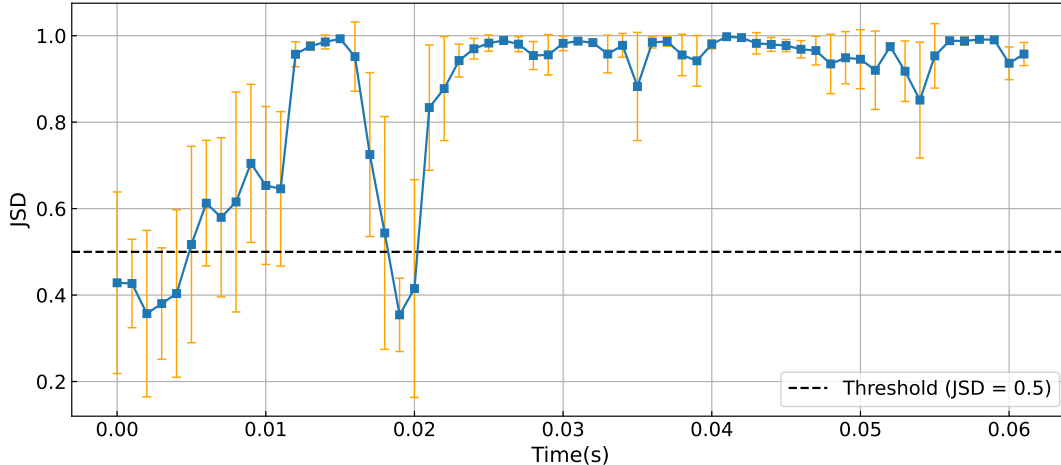


FIG. 3. The JSD values between posterior distributions obtained from data contaminated with glitches and those from clean data at the time point of noise insertion. The data points in the graph are the mean JSD calculated from five independent runs. Error bars represent the standard deviation (SD) of these five runs. The horizontal dashed line indicates a threshold of $JSD = 0.5$, above which the posterior deviation is considered significant.

are roughly the same. However, the marginal distribution of phase shows the opposite trend, with lower JSD near the tail.

2. The SNR of glitches

Next, we discuss the effect of the SNR of glitches on model posterior inference. We inject glitches at the center of the ringdown signal, specifically at $t = 0.05$ seconds. Figure 5 shows that with increasing glitch SNR, the difference between the posterior distributions of the model and those without noise increases, making the model inference gradually unreliable.

Under lower SNR conditions, the glitch primarily acts as a background perturbation, and its influence can be partially absorbed by the model's ability to approximate complex distributions. In contrast, under higher SNR conditions, the energy of the glitch approaches or even exceeds that of the main signal, causing the glitch to overlap with the signal modes in the time-frequency domain, thereby confusing mode identification and separation. It has a particularly significant effect on amplitude-dependent and phase-dependent parameters.

It is worth knowing that although the overall JSD increases with increasing SNR, its growth rate tends to flatten after $SNR > 20$. This suggests that even under conditions of strong glitches, key parameters like mass and spin remain relatively stable. This inferential stability likely arises because these parameters are primarily determined by the signal's frequency structure, which itself is robust to strong noise.

Similarly to the injection time test in chapter III B 1, we also measure the JSD of marginal distributions as

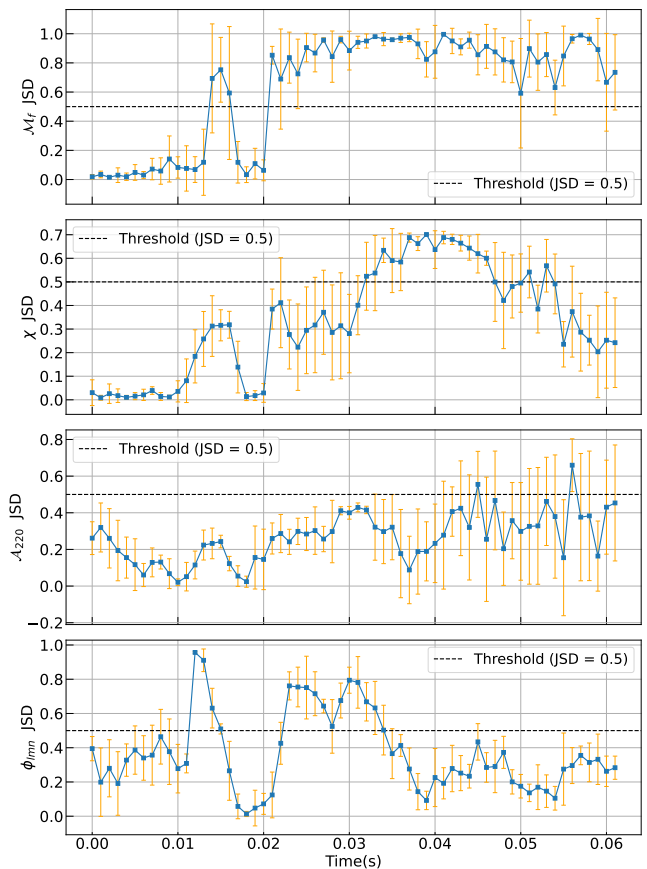


FIG. 4. The JSD value of marginal distribution different time point between posterior distributions obtained from data contaminated with glitches and those from clean data at the time point of noise insertion. The same JSD threshold as in Fig. 3 is shown for reference.

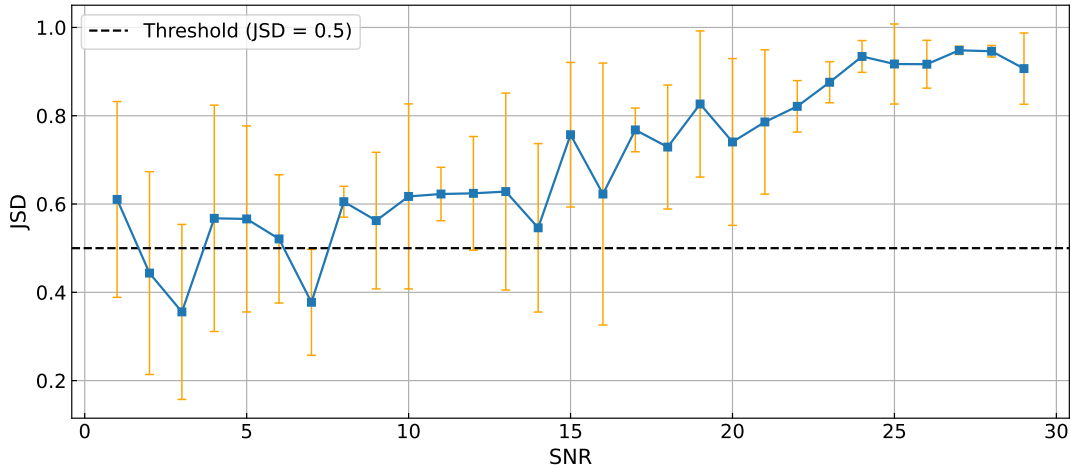


FIG. 5. The JSD value between posterior distributions obtained from data contaminated with glitches and those from clean data for different glitches SNR. The data points in the graph are the mean JSD calculated from five independent runs. Error bars represent the SD of these five runs. The same JSD threshold as in Fig. 3 is shown for reference.

shown in Fig. 6 below. Overall, all marginal distributions have low JSD values. The JSD trend for mass matches the overall JSD trend, whereas the JSD values for spin and phase parameters show weaker dependence on SNR. However, the marginal distribution of amplitude shows the opposite trend, with lower JSD at the high SNR. Therefore, we can draw a conclusion that the glitch SNR has a lower impact on the value of JSD than the injection time of glitches.

IV. CONCLUSION

This study aims to develop and evaluate a likelihood-free method for estimating parameters of GW ringdown signals in the time domain. We focus on its performance under both ideal conditions and non-Gaussian noise interference. By integrating amortized NPE with normalizing flows, we construct an efficient Bayesian inference framework. Using this framework, we systematically evaluate how glitches affect the inference results.

The main findings of this study can be summarized in two key areas. Firstly, performance validation on clean data: When sufficiently trained, the amortized NPE model can produce posterior distributions that are statistically consistent with those from classical MCMC methods. Through corner plot comparisons, the KS test, and coverage probability analyses, we have confirmed the model's reliability in terms of parameter recovery capability and statistical calibration. At the same time, the model achieves computational speed-ups of several orders of magnitude, providing a viable solution for processing the high event rates expected from next-generation GW detectors. Secondly, robustness analysis on noise-contaminated data: We have provided systematic quan-

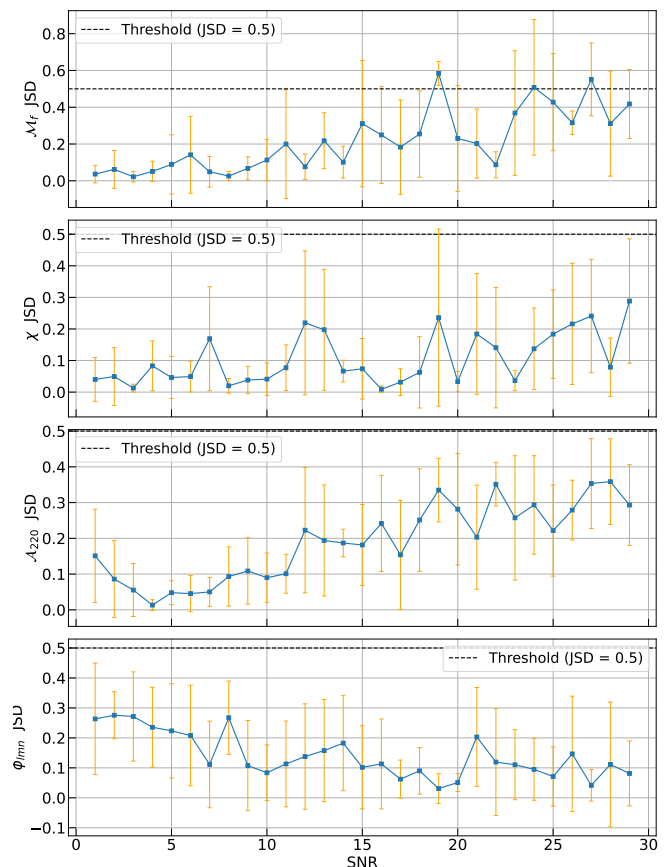


FIG. 6. The JSD value of different SNR marginal distribution between posterior distributions obtained from data contaminated with glitches and those from clean data at the time point of noise insertion. The same JSD threshold as in Fig. 3 is shown for reference.

tification of the mechanisms through which glitches affect model performance. Our analysis reveals key findings on how glitches affect inference. Firstly, the injection time of a glitch has a decisive influence on inference bias. Glitches that overlap with the late, information-poor portion of the signal cause significant parameter estimation deviations. Secondly, glitch strength correlates positively with inference error. However, this impact remains limited under low SNR conditions. Thirdly, different physical parameters show varying sensitivities to glitches. Mass and spin parameters are the most affected.

While this study has achieved significant results, several limitations remain and point to promising directions for future research. The current work is primarily based on a simplified single-mode signal model ($Kerr_{2,2,0}$) and has not yet been extended to complete waveforms incorporating higher order QNM. Secondly, the experiments employ simulated glitches whose waveforms may differ from transient noise in real detectors. Finally, model training relies heavily on extensive simulated data and is sensitive to the accuracy of both the waveform and noise models.

This study holds significant value in both methodological and applied contexts. Methodologically, we have systematically applied amortized NPE to time-domain GW ringdown analysis for the first time and established a comprehensive performance evaluation framework.

The experimental results of this study indicate that the amortized SBI framework achieves statistical reliability comparable to classical methods under ideal conditions, while significantly improving computational efficiency. More importantly, we systematically reveal the mechanisms through which non-Gaussian noise, especially glitches, affects parameter estimation: the influence of temporal location outweighs that of strength, and different parameters have varying sensitivities to noise. Therefore, this work lays a foundation for developing noise-resistant inference pipelines in the future. We suggest implementing stronger data quality control or model attention mechanisms when signal information is sparse, such as during the ringdown tail.

Future work could extend in the following directions. First, integrating multimodal signal models to extend the framework to complete ringdown waveforms that in-

clude higher order QNM; Second, developing adaptive noise-resistant training strategies, such as dynamically injecting real detector noise characteristics into training data to enhance the model’s generalization to complex noise environments; Third, promoting the application of the method in real-time data processing systems to provide efficient tools for online parameter inference in next-generation GW detectors.

The research not only indicates the statistical reliability of the method but, more importantly, reveals how the accuracy of parameter estimation varies when the method encounters transient noise interference (such as simulated glitches). This provides an important reference for the practical application of likelihood-free inference in GW data analysis. In practical terms, the developed inference framework offers an efficient tool for handling the high SNR observations expected from next-generation GW detectors. Furthermore, this framework can be extended to other cosmological and astronomical fields facing similar challenges, providing new approaches for addressing parameter estimation problems in complex noise environments.

ACKNOWLEDGMENTS

We thank the developers of the open-source software packages used in this work, including `lampe`, `Pycbc`, `pyRing`, and `cpnest`, which were essential for the implementation and validation of our inference framework. This research has made use of data or software obtained from the Gravitational Wave Open Science Center (gwosc.org), a service of LIGO Laboratory, the LIGO Scientific Collaboration, the Virgo Collaboration, and KAGRA. This work is supported by the National Natural Science Foundation of China (Grants Nos. 12473001, 12575049, and 12533001), the National SKA Program of China (Grants Nos. 2022SKA0110200 and 2022SKA0110203), the China Manned Space Program (Grant No. CMS-CSST-2025-A02), the National 111 Project (Grant No. B16009), and the China Scholarship Council.

-
- [1] B. Abbott, R. Abbott, T. Abbott, M. Abernathy, F. Acernese, *et al.*, *Physical Review Letters* **116** (2016), [10.1103/physrevlett.116.061102](https://arxiv.org/abs/10.1103/physrevlett.116.061102).
 - [2] B. Abbott, R. Abbott, T. Abbott, S. Abraham, *et al.*, *Physical Review X* **9** (2019), [10.1103/physrevx.9.031040](https://arxiv.org/abs/10.1103/physrevx.9.031040).
 - [3] R. Abbott, T. Abbott, S. Abraham, F. Acernese, K. Ackley, A. Adams, C. Adams, R. Adhikari, V. Adya, C. Affeldt, M. Agathos, *et al.*, *Physical Review X* **11** (2021), [10.1103/physrevx.11.021053](https://arxiv.org/abs/10.1103/physrevx.11.021053).
 - [4] T. L. S. Collaboration, the Virgo Collaboration, R. Abbott, *et al.*, “Gwtc-2.1: Deep extended catalog of compact binary coalescences observed by ligo and virgo during the first half of the third observing run,” (2022), [arXiv:2108.01045 \[gr-qc\]](https://arxiv.org/abs/2108.01045).
 - [5] R. Abbott, T. Abbott, F. Acernese, K. Ackley, C. Adams, *et al.*, *Physical Review X* **13** (2023), [10.1103/physrevx.13.041039](https://arxiv.org/abs/10.1103/physrevx.13.041039).
 - [6] A. G. Abac, I. Aboueffetouh, F. Acernese, K. Ackley, *et al.*, “Gwtc-4.0: Updating the gravitational-wave transient catalog with observations from the first part of the fourth ligo-virgo-kagra observing run,” (2025),

- arXiv:2508.18082 [gr-qc].
- [7] S. A. Teukolsky, *Astrophys. J.* **185**, 635 (1973).
- [8] B. F. Schutz, *Nature* **323**, 310 (1986).
- [9] D. E. Holz and S. A. Hughes, *The Astrophysical Journal* **629**, 15–22 (2005).
- [10] B. S. Sathyaprakash and B. F. Schutz, *Living Reviews in Relativity* **12** (2009), 10.12942/lrr-2009-2.
- [11] F. Acernese, M. Agathos, K. Agatsuma, D. Aisa, N. Allemandou, A. Allocca, *et al.*, *Classical and Quantum Gravity* **32**, 024001 (2014).
- [12] J. Aasi, B. P. Abbott, R. Abbott, T. Abbott, M. R. Abernathy, *et al.*, *Classical and Quantum Gravity* **32**, 074001 (2015).
- [13] B. Abbott, R. Abbott, T. Abbott, F. Acernese, K. Ackley, *et al.*, *Physical Review Letters* **121** (2018), 10.1103/physrevlett.121.161101.
- [14] E. Annala, T. Gorda, A. Kurkela, and A. Vuorinen, *Physical Review Letters* **120** (2018), 10.1103/physrevlett.120.172703.
- [15] L.-F. Wang, X.-N. Zhang, J.-F. Zhang, and X. Zhang, *Physics Letters B* **782**, 87–93 (2018).
- [16] G. Chen, L. Zhang, W.-H. Zhang, X.-X. Peng, L. Xu, Z.-D. Liu, X.-Y. Xu, J.-S. Tang, Y.-N. Sun, D.-Y. He, J.-S. Xu, Z.-Q. Zhou, C.-F. Li, and G.-C. Guo, *Phys. Rev. Lett.* **121**, 060506 (2018).
- [17] B. Abbott, R. Abbott, T. Abbott, F. Acernese, K. Ackley, *et al.*, *Physical Review Letters* **123** (2019), 10.1103/physrevlett.123.011102.
- [18] E. Berti, V. Cardoso, and A. O. Starinets, *Classical and Quantum Gravity* **26**, 163001 (2009).
- [19] E. Berti, E. Barausse, V. Cardoso, L. Gualtieri, P. Pani, U. Sperhake, L. C. Stein, N. Wex, K. Yagi, T. Baker, C. P. Burgess, F. S. Coelho, D. Doneva, A. D. Felice, P. G. Ferreira, P. C. C. Freire, J. Healy, C. Herdeiro, M. Horbatsch, B. Kleihaus, A. Klein, K. Kokkotas, J. Kunz, P. Laguna, R. N. Lang, T. G. F. Li, T. Lit-tenberg, A. Matas, S. Mirshekari, H. Okawa, E. Radu, R. O’Shaughnessy, B. S. Sathyaprakash, C. V. D. Broeck, H. A. Winther, H. Witek, M. E. Aghili, J. Als-ing, B. Bolen, L. Bombelli, S. Caudill, L. Chen, J. C. Degollado, R. Fujita, C. Gao, D. Gerosa, S. Kamali, H. O. Silva, J. G. Rosa, L. Sadeghian, M. Sampaio, H. Sotani, and M. Zilhao, *Classical and Quantum Grav-ity* **32**, 243001 (2015).
- [20] E. Berti, V. Cardoso, J. A. Gonzalez, U. Sperhake, M. Hannam, S. Husa, and B. Brügmann, *Phys. Rev. D* **76**, 064034 (2007).
- [21] M. Lagos, T. Andrade, J. Rafecas-Ventosa, and L. Hui, (2024), 10.48550/ARXIV.2411.02264.
- [22] C. Cutler and a. E. Flanagan, *Physical Review D* **49**, 2658–2697 (1994).
- [23] R.-Y. Guo, J.-F. Zhang, and X. Zhang, *Journal of Cosmology and Astroparticle Physics* **2019**, 054–054 (2019).
- [24] R. Abbott, H. Abe, F. Acernese, K. Ackley, N. Adhikari, *et al.*, *The Astrophysical Journal* **949**, 76 (2023).
- [25] G. Engelhardt, A. Bhoonah, and W. V. Liu, “Detecting axion dark matter with rydberg atoms via induced electric dipole transitions,” (2023), arXiv:2304.05863 [hep-ph].
- [26] J.-Y. Song, J.-Z. Qi, J.-F. Zhang, and X. Zhang, *Astrophys. J. Lett.* **985**, L44 (2025), arXiv:2503.10346 [astro-ph.CO].
- [27] S.-J. Jin, J.-Y. Song, T.-Y. Sun, S.-R. Xiao, H. Wang, L.-F. Wang, J.-F. Zhang, and X. Zhang, *Sci. China Phys. Mech. Astron.* **69**, 220401 (2026), arXiv:2507.12965 [astro-ph.CO].
- [28] N. Muttoni, A. Mangiagli, A. Sesana, D. Laghi, W. Del Pozzo, D. Izquierdo-Villalba, and M. Rosati, *Physical Review D* **105** (2022), 10.1103/phys-revd.105.043509.
- [29] E. Berti, V. Cardoso, and C. M. Will, *Physical Review D* **73** (2006), 10.1103/physrevd.73.064030.
- [30] Z. Zhang, S. Li, X.-D. Li, X. Zhang, and M. Li, *JCAP* **06**, 009 (2012), arXiv:1204.6135 [astro-ph.CO].
- [31] J.-F. Zhang, M.-M. Zhao, Y.-H. Li, and X. Zhang, *JCAP* **04**, 038 (2015), arXiv:1502.04028 [astro-ph.CO].
- [32] R.-Y. Guo and X. Zhang, *Eur. Phys. J. C* **76**, 163 (2016), arXiv:1512.07703 [astro-ph.CO].
- [33] B. P. Abbott, R. Abbott, T. D. Abbott, F. Acernese, K. Ackley, *et al.*, *Nature* **551**, 85–88 (2017).
- [34] L. Barack and A. Pound, *Reports on Progress in Physics* **82**, 016904 (2018).
- [35] R.-Y. Guo, J.-F. Zhang, and X. Zhang, *JCAP* **02**, 054 (2019), arXiv:1809.02340 [astro-ph.CO].
- [36] M. Soares-Santos, A. Palmese, W. Hartley, J. An-nis, *et al.*, *The Astrophysical Journal Letters* **876**, L7 (2019).
- [37] K. Hotokezaka, E. Nakar, O. Gottlieb, S. Nissanke, K. Masuda, G. Hallinan, K. P. Mooley, and A. T. Deller, *Nature Astronomy* **3**, 940 (2019).
- [38] J.-F. Zhang, M. Zhang, S.-J. Jin, J.-Z. Qi, and X. Zhang, *Journal of Cosmology and Astroparticle Physics* **2019**, 068–068 (2019).
- [39] M. Fishbach, R. Gray, I. M. Hernandez, H. Qi, A. Sur, *et al.*, *The Astrophysical Journal Letters* **871**, L13 (2019).
- [40] J.-F. Zhang, L.-Y. Gao, D.-Z. He, and X. Zhang, *Physics Letters B* **799**, 135064 (2019).
- [41] B. P. Abbott, R. Abbott, T. D. Abbott, S. Abraham, *et al.*, *The Astrophysical Journal* **909**, 218 (2021).
- [42] T.-N. Li, Y.-H. Li, G.-H. Du, P.-J. Wu, L. Feng, J.-F. Zhang, and X. Zhang, *Eur. Phys. J. C* **85**, 608 (2025), arXiv:2411.08639 [astro-ph.CO].
- [43] T. L. S. Collaboration, the Virgo Collaboration, the KAGRA Collaboration, A. G. Abac, I. Abouelfet-touh, F. Acernese, K. Ackley, *et al.*, “Gwtc-4.0: Constraints on the cosmic expansion rate and modified gravitational-wave propagation,” (2025), arXiv:2509.04348 [astro-ph.CO].
- [44] J.-Y. Song, G.-H. Du, T.-N. Li, L.-F. Wang, J.-Z. Qi, J.-F. Zhang, and X. Zhang, (2025), arXiv:2511.12017 [astro-ph.CO].
- [45] P. Amaro-Seoane, H. Audley, S. Babak, J. Baker, E. Barausse, P. Bender, E. Berti, P. Binetruy, M. Born, D. Bortoluzzi, *et al.*, arXiv preprint arXiv:1702.00786 (2017).
- [46] Y.-X. Zhang, T.-Y. Sun, C.-Y. Xiong, S.-T. Liu, Y.-X. Wang, S.-J. Jin, J.-F. Zhang, and X. Zhang, “Factorized neural posterior estimation for rapid and reliable inference of parameterized post-einsteinian deviation parameters in gravitational waves,” (2026), arXiv:2602.01319 [astro-ph.IM].
- [47] X. Zhang and Y. Ling, *JCAP* **08**, 012 (2007), arXiv:0705.2656 [gr-qc].
- [48] Q.-H. Zhu, Z.-C. Zhao, S. Wang, and X. Zhang, *Chin. Phys. C* **48**, 125105 (2024), arXiv:2307.13574 [astro-ph.CO].

- [49] Y.-H. Li, S. Wang, X.-D. Li, and X. Zhang, *JCAP* **02**, 033 (2013), [arXiv:1207.6679 \[astro-ph.CO\]](#).
- [50] L. Feng and X. Zhang, *JCAP* **08**, 072 (2016), [arXiv:1607.05567 \[astro-ph.CO\]](#).
- [51] I. Gat, H. van Eerten, and A. MacFadyen, *The Astrophysical Journal* **773**, 2 (2013).
- [52] A. Iovino, S. Matarrese, G. Perna, A. Ricciardone, and A. Riotto, *Physics Letters B* **872**, 140039 (2026).
- [53] B. P. Abbott, R. Abbott, T. D. Abbott, S. Abraham, F. Acernese, *et al.*, *Living Reviews in Relativity* **23**, 3 (2020).
- [54] F. Pretorius, *Physical Review Letters* **95** (2005), [10.1103/physrevlett.95.121101](#).
- [55] D. George and E. Huerta, *Physics Letters B* **778**, 64 (2018).
- [56] M. Boyle, D. Hemberger, D. A. B. Iozzo, G. Lovelace, S. Ossokine, H. P. Pfeiffer, M. A. Scheel, L. C. Stein, C. J. Woodford, A. B. Zimmerman, N. Afshari, K. Barkett, J. Blackman, K. Chatziioannou, T. Chu, N. Demos, N. Deppe, S. E. Field, N. L. Fischer, E. Foley, H. Fong, A. Garcia, M. Giesler, F. Hebert, I. Hinder, R. Katebi, H. Khan, L. E. Kidder, P. Kumar, K. Kuper, H. Lim, M. Okounkova, T. Ramirez, S. Rodriguez, H. R. Rüter, P. Schmidt, B. Szilagyi, S. A. Teukolsky, V. Varma, and M. Walker, *Classical and Quantum Gravity* **36**, 195006 (2019).
- [57] P. G. Krastev, K. Gill, V. A. Villar, and E. Berger, *Physics Letters B* **815**, 136161 (2021).
- [58] R. Qiu, P. G. Krastev, K. Gill, and E. Berger, *Physics Letters B* **840**, 137850 (2023).
- [59] H. V. Peiris, “Considerations in the interpretation of cosmological anomalies,” (2014), [arXiv:1410.3837 \[astro-ph.CO\]](#).
- [60] V. Cesare, A. Diaferio, T. Matsakos, and G. Angus, *Astronomy & Astrophysics* **637**, A70 (2020).
- [61] K. Xu, M. Zhang, S. Jegelka, and K. Kawaguchi, “Optimization of graph neural networks: Implicit acceleration by skip connections and more depth,” (2021), [arXiv:2105.04550 \[cs.LG\]](#).
- [62] X. Fan, J. Li, X. Li, Y. Zhong, and J. Cao, *Science China Physics, Mechanics & Astronomy* **62** (2019), [10.1007/s11433-018-9321-7](#).
- [63] A. J. Chua and M. Vallisneri, *Physical Review Letters* **124** (2020), [10.1103/physrevlett.124.041102](#).
- [64] H. Gabbard, C. Messenger, I. S. Heng, F. Tonolini, and R. Murray-Smith, *Nature Physics* **18**, 112–117 (2021).
- [65] W. Wei, A. Khan, E. Huerta, X. Huang, and M. Tian, *Physics Letters B* **812**, 136029 (2021).
- [66] Y. Xu, M. Du, P. Xu, B. Liang, and H. Wang, *Physics Letters B* **858**, 139016 (2024).
- [67] J. R. Gair, S. Deng, and S. Babak, “Contamination of transient gravitational waves in lisa data by gaps and glitches,” (2025), [arXiv:2510.16770 \[gr-qc\]](#).
- [68] C.-Y. Xiong, T.-Y. Sun, J.-F. Zhang, and X. Zhang, *Physical Review D* **111** (2025), [10.1103/physrevd.111.024019](#).
- [69] A. G. Abac, I. Abouelfettouh, F. Acernese, K. Ackley, C. Adamcewicz, *et al.*, “Constraints on gravitational waves from the 2024 vela pulsar glitch,” (2026), [arXiv:2512.17990 \[gr-qc\]](#).
- [70] A. G. Abac, I. Abouelfettouh, F. Acernese, K. Ackley, *et al.* (The LIGO Scientific Collaboration, The Virgo Collaboration, and The KAGRA Collaboration), *Phys. Rev. Lett.* **136**, 041403 (2026).
- [71] B. P. Abbott, R. Abbott, T. D. Abbott, S. Abraham, F. Acernese, *et al.*, *Classical and Quantum Gravity* **37**, 055002 (2020).
- [72] J. Wurster, M. R. Bate, D. J. Price, and I. A. Bonnell, *Monthly Notices of the Royal Astronomical Society* **511**, 746–764 (2022).
- [73] B. Allen, *Phys. Rev. D* **105**, 102003 (2022).
- [74] R. Cotesta, G. Carullo, E. Berti, and V. Cardoso, *Phys. Rev. Lett.* **129**, 111102 (2022).
- [75] H. Gabbard, M. Williams, F. Hayes, and C. Messenger, *Phys. Rev. Lett.* **120**, 141103 (2018).
- [76] D. Wei, Y. Li, Y. Wang, T. Qian, Y. Zheng, and Z. Liu, in *Medical Imaging 2020: Computer-Aided Diagnosis*, edited by H. K. Hahn and M. A. Mazurowski (SPIE, 2020) p. 91.
- [77] E. Cuoco, J. Powell, M. Cavaglià, K. Ackley, M. Berger, C. Chatterjee, M. Coughlin, S. Coughlin, P. Easter, R. Essick, H. Gabbard, T. Gebhard, S. Ghosh, L. Haegel, A. Iess, D. Keitel, Z. Márka, S. Márka, F. Morawski, T. Nguyen, R. Ormiston, M. Pürrer, M. Razzano, K. Staats, G. Vajente, and D. Williams, *Machine Learning: Science and Technology* **2**, 011002 (2020).
- [78] C. Pacilio, S. Bhagwat, and R. Cotesta, *Physical Review D* **110** (2024), [10.1103/physrevd.110.083010](#).
- [79] M. Punturo, M. Abernathy, F. Acernese, B. Allen, N. Andersson, *et al.*, *Classical and Quantum Gravity* **27**, 194002 (2010).
- [80] B. P. Abbott, R. Abbott, T. D. Abbott, M. R. Abernathy, K. Ackley, C. Adams, *et al.*, *Classical and Quantum Gravity* **34**, 044001 (2017).
- [81] E. D. Hall, *Galaxies* **10**, 90 (2022).
- [82] M. Pieroni, A. Ricciardone, and E. Barausse, *Scientific Reports* **12** (2022), [10.1038/s41598-022-19540-7](#).
- [83] D. George and E. A. Huerta, *Phys. Rev. D* **97**, 044039 (2018).
- [84] M. Dax, S. R. Green, J. Gair, J. H. Macke, A. Buonanno, and B. Schölkopf, *Physical Review Letters* **127** (2021), [10.1103/physrevlett.127.241103](#).
- [85] M. Dax, S. R. Green, J. Gair, N. Gupte, M. Pürrer, V. Raymond, J. Wildberger, J. H. Macke, A. Buonanno, and B. Schölkopf, *Nature* **639**, 49–53 (2025).
- [86] H. Xia, L. Shao, J. Zhao, and Z. Cao, *Physical Review D* **103** (2021), [10.1103/physrevd.103.024040](#).
- [87] S. Jadhav, N. Mukund, B. Gadre, S. Mitra, and S. Abraham, *Physical Review D* **104** (2021), [10.1103/physrevd.104.064051](#).
- [88] J. A. Dror, B. V. Lehmann, H. H. Patel, and S. Profumo, *Phys. Rev. D* **104**, 083021 (2021).
- [89] E. Cuoco, B. Patricelli, A. Iess, and F. Morawski, *Nature Computational Science* **2**, 479 (2022).
- [90] Y. Zhang, H. Xu, M. Liu, C. Liu, Y. Zhao, and J. Zhu, *Phys. Rev. D* **106**, 122002 (2022).
- [91] C. Ma, W. Wang, H. Wang, and Z. Cao, *Physical Review D* **105** (2022), [10.1103/physrevd.105.083013](#).
- [92] M. B. Schäfer, O. Zelenka, A. H. Nitz, F. Ohme, and B. Brügmann, *Physical Review D* **105** (2022), [10.1103/physrevd.105.043002](#).
- [93] P. Nousi, A. E. Koloniari, N. Passalis, P. Iosif, N. Stergioulas, and A. Tefas, *Physical Review D* **108** (2023), [10.1103/physrevd.108.024022](#).
- [94] T. Zhao, R. Lyu, H. Wang, Z. Cao, and Z. Ren, *Communications Physics* **6** (2023), [10.1038/s42005-023-01334-6](#).

- [95] Q. Yun, W.-B. Han, Y.-Y. Guo, H. Wang, and M. Du, “The detection, extraction and parameter estimation of extreme-mass-ratio inspirals with deep learning,” (2023), [arXiv:2311.18640 \[gr-qc\]](#).
- [96] C. Ma, W. Wang, H. Wang, and Z. Cao, *Phys. Rev. D* **107**, 063029 (2023).
- [97] A. Trovato, E. Chassande-Mottin, M. Bejger, R. Flamar, and N. Courty, *Classical and Quantum Gravity* **41**, 125003 (2024).
- [98] N. Stergioulas, “Machine learning applications in gravitational wave astronomy,” (2024), [arXiv:2401.07406 \[gr-qc\]](#).
- [99] A. McLeod, D. Beveridge, L. Wen, and A. Wicenc, *Physical Review D* **111** (2025), [10.1103/physrevd.111.024035](#).
- [100] K. Cranmer, J. Brehmer, and G. Louppe, *Proceedings of the National Academy of Sciences* **117**, 30055 (2020).
- [101] J. Hermans, V. Begy, and G. Louppe, “Likelihood-free mcmc with amortized approximate ratio estimators,” (2020), [arXiv:1903.04057 \[stat.ML\]](#).
- [102] M. Dax, S. R. Green, J. Gair, J. H. Macke, A. Buonanno, and B. Schölkopf, *Phys. Rev. Lett.* **127**, 241103 (2021).
- [103] Y.-X. Wang, X. Wei, C.-Y. Li, T.-Y. Sun, S.-J. Jin, H. Wang, J.-L. Cui, J.-F. Zhang, and X. Zhang, *Phys. Rev. D* **112**, 024030 (2025), [arXiv:2410.20129 \[gr-qc\]](#).
- [104] P. G. Krastev, *Physics Letters B* **803**, 135330 (2020).
- [105] M. Dax, S. R. Green, J. Gair, J. H. Macke, A. Buonanno, and B. Schölkopf, *Physical Review Letters* **127** (2021), [10.1103/physrevlett.127.241103](#).
- [106] U. Bhardwaj, J. Alvey, B. K. Miller, S. Nissanke, and C. Weniger, *Physical Review D* **108** (2023), [10.1103/physrevd.108.042004](#).
- [107] T. Wouters, P. T. Pang, T. Dietrich, and C. Van Den Broeck, *Physical Review D* **110** (2024), [10.1103/physrevd.110.083033](#).
- [108] S. R. Green and J. Gair, “Complete parameter inference for gw150914 using deep learning,” (2020), [arXiv:2008.03312 \[astro-ph.IM\]](#).
- [109] T. S. Yamamoto and T. Tanaka, (2020), [10.48550/ARXIV.2002.12095](#).
- [110] D. P. Kingma and M. Welling, “Auto-encoding variational bayes,” (2022), [arXiv:1312.6114 \[stat.ML\]](#).
- [111] T.-Y. Sun, T.-N. Li, H. Wang, J.-F. Zhang, and X. Zhang, (2025), [arXiv:2510.27086 \[astro-ph.CO\]](#).
- [112] G. Papamakarios and I. Murray, “Fast ϵ -free inference of simulation models with bayesian conditional density estimation,” (2018), [arXiv:1605.06376 \[stat.ML\]](#).
- [113] Z. Qin, T.-Y. Sun, B.-Y. Li, J.-F. Zhang, X. Guo, and X. Zhang, (2025), [arXiv:2505.20996 \[gr-qc\]](#).
- [114] F. Feroz, M. P. Hobson, and M. Bridges, *Monthly Notices of the Royal Astronomical Society* **398**, 1601 (2009).
- [115] A. Kolmus, J. Janquart, T. Baka, T. van Laarhoven, C. V. D. Broeck, and T. Heskes, (2024), [10.48550/ARXIV.2403.02443](#).
- [116] K. He, X. Zhang, S. Ren, and J. Sun, (2015).
- [117] J. Hermans, A. Delaunoy, F. Rozet, A. Wehenkel, V. Begy, and G. Louppe, “A trust crisis in simulation-based inference? your posterior approximations can be unfaithful,” (2022), [arXiv:2110.06581 \[stat.ML\]](#).
- [118] C. Bishop, *Pattern Recognition and Machine Learning* (Stat Sci, 2006).
- [119] E. Tabak and E. Vanden-Eijnden, *Communications in Mathematical Sciences - COMMUN MATH SCI* **8** (2010), [10.4310/CMS.2010.v8.n1.a11](#).
- [120] E. Tabak and T. Cristina, *Communications on Pure and Applied Mathematics* **66** (2013), [10.1002/cpa.21423](#).
- [121] T.-Y. Sun, C.-Y. Xiong, S.-J. Jin, Y.-X. Wang, J.-F. Zhang, and X. Zhang, *Chin. Phys. C* **48**, 045108 (2024), [arXiv:2312.08122 \[gr-qc\]](#).
- [122] T.-Y. Sun, Y. Shao, Y. Li, Y. Xu, H. Wang, and X. Zhang, *Commun. Phys.* **8**, 220 (2025), [arXiv:2407.14298 \[astro-ph.CO\]](#).
- [123] S. T. Radev, M. Schmitt, L. Schumacher, L. Elsemüller, V. Pratz, Y. Schälte, U. Köthe, and P.-C. Bürkner, “Bayesflow: Amortized bayesian workflows with neural networks,” (2023), [arXiv:2306.16015 \[cs.LG\]](#).
- [124] A. Zammit-Mangion, M. Sainsbury-Dale, and R. Huser, *Annual Review of Statistics and Its Application* **12**, 311 (2025).
- [125] C. Hahn and P. Melchior, *The Astrophysical Journal* **938**, 11 (2022).
- [126] A. Kolmus, J. Janquart, T. Baka, T. van Laarhoven, C. V. D. Broeck, and T. Heskes, “Tuning neural posterior estimation for gravitational wave inference,” (2024), [arXiv:2403.02443 \[astro-ph.IM\]](#).
- [127] P. Jaranowski, A. Królak, and B. F. Schutz, *Phys. Rev. D* **58**, 063001 (1998).
- [128] M. Isi, M. Giesler, W. M. Farr, M. A. Scheel, and S. A. Teukolsky, *Phys. Rev. Lett.* **123**, 111102 (2019).
- [129] G. Papamakarios, E. Nalisnick, D. J. Rezende, S. Mohamed, and B. Lakshminarayanan, “Normalizing flows for probabilistic modeling and inference,” (2021), [arXiv:1912.02762 \[stat.ML\]](#).
- [130] M. Isi, M. Giesler, W. M. Farr, M. A. Scheel, and S. A. Teukolsky, *Physical Review Letters* **123** (2019), [10.1103/physrevlett.123.111102](#).
- [131] G. Carullo, W. Del Pozzo, and J. Veitch, *Physical Review D* **99** (2019), [10.1103/physrevd.99.123029](#).
- [132] R. Abbott, T. Abbott, S. Abraham, F. Acernese, K. Ackley, *et al.*, *Physical Review D* **103** (2021), [10.1103/physrevd.103.122002](#).
- [133] G. Carullo, W. Del Pozzo, and J. Veitch, “pyRing: a time-domain ringdown analysis python package,” [git.ligo.org/lscsoft/pyring](#) (2023).
- [134] R. H. C. Lopes, “Kolmogorov-smirnov test,” in *International Encyclopedia of Statistical Science*, edited by M. Lovric (Springer Berlin Heidelberg, Berlin, Heidelberg, 2011) pp. 718–720.
- [135] T. Sidery *et al.*, *Phys. Rev. D* **89**, 084060 (2014), [arXiv:1312.6013 \[astro-ph.IM\]](#).
- [136] J. Veitch *et al.*, *Phys. Rev. D* **91**, 042003 (2015), [arXiv:1409.7215 \[gr-qc\]](#).
- [137] C. M. Biwer, C. D. Capano, S. De, M. Cabero, D. A. Brown, A. H. Nitz, and V. Raymond, *Publ. Astron. Soc. Pac.* **131**, 024503 (2019), [arXiv:1807.10312 \[astro-ph.IM\]](#).
- [138] E. Thrane and C. Talbot, *Publications of the Astronomical Society of Australia* **36** (2019), [10.1017/pasa.2019.2](#).
- [139] L. Yu, K. Metwaly, J. Z. Wang, and V. Monga, “Surface defect detection and evaluation for marine vessels using multi-stage deep learning,” (2022), [arXiv:2203.09580 \[cs.CV\]](#).
- [140] S. Talts, M. Betancourt, D. Simpson, A. Vehtari, and A. Gelman, “Validating bayesian inference algorithms with simulation-based calibration,” (2020), [arXiv:1804.06788 \[stat.ME\]](#).

- [141] K. Karchev, R. Trotta, and C. Weniger, *Monthly Notices of the Royal Astronomical Society* **520**, 1056–1072 (2022).
- [142] C. R. Rao, *Differential geometry in statistical inference* **10**, 217 (1987).
- [143] J. Lin, *IEEE Transactions on Information Theory* **37**, 145 (1991).
- [144] S. Kullback and R. A. Leibler, *The Annals of Mathematical Statistics* **22**, 79 (1951).
- [145] I. Csiszar, *The Annals of Probability* **3**, 146 (1975).
- [146] I. M. Romero-Shaw *et al.*, *Mon. Not. Roy. Astron. Soc.* **499**, 3295 (2020), [arXiv:2006.00714](https://arxiv.org/abs/2006.00714) [astro-ph.IM].
- [147] R. Macas, J. Pooley, L. K. Nuttall, D. Davis, M. J. Dyer, Y. Lecoeuche, J. D. Lyman, J. McIver, and K. Rink, *Physical Review D* **105** (2022), 10.1103/physrevd.105.103021.